

Phase-tunable multiple Andreev reflections in a quantum spin Hall strip

Xue Yang,¹ Pablo Buset,² and Bo Lu¹

¹*Department of Physics, Tianjin University, Tianjin 300072, China*

²*Department of Theoretical Condensed Matter Physics, Condensed Matter Physics Center (IFIMAC) and Instituto Nicolás Cabrera, Universidad Autónoma de Madrid, 28049 Madrid, Spain*

(Dated: January 24, 2023)

A quantum spin Hall strip where different edges are contacted by s -wave superconductors with a phase difference ϕ supports Majorana Kramers pairs (MKPs). We study the transport properties of this setup in a four-terminal normal metal (N)/insulator (I)/superconductor (S) and S/I/S junction. The tunneling spectroscopy for the N/I/S junction reveals that the signature of MKPs is that the conductance is quantized by $4e^2/h$ at zero bias and suppressed at the gap edges. In the S/I/S junction, the subharmonic gap structure displays a phase-tuned even-odd effect, where all odd spikes disappear in the presence of MKPs and the remaining even spikes split when superconductors forming the junction have different gaps. We explain these features by showing that midgap bound states enhance the transmission of the even order multiple Andreev reflections, while the reduced density of states at the gap edges suppresses the odd order ones.

I. INTRODUCTION.

The quantum spin Hall insulator (QSHI) [1–6] is a prominent topological material that is recently attracting significant attention. Its defining feature is the emergence of helical, or spin-momentum locked, edge states where different spins circulate in opposite directions. These helical edge states have been measured in experiments [7, 8] and provide a pathway to develop novel quantum phenomena and functionalities [9]. For example, QSHIs are predicted to host Majorana bound states (MBSs) with revolutionary prospects in fault-tolerant quantum computations [10–18]. Topological superconductivity can be generated in helical states with or without time-reversal invariance. Breaking time-reversal symmetry, a single helical edge is proximitized by a ferromagnet (F) and a superconductor (S) and MBSs appear at the boundaries of the F/S or S/F/S junctions [19–21]. Combining ferromagnets and superconductors in QSHIs is experimentally challenging; therefore, efforts are devoted to realize time-reversal invariant Majorana Kramers pairs (MKPs).

In one approach, the two opposite edges of a QSHI strip are coupled to superconducting leads with a phase difference of π [22, 23]. An experimental signature to detect MKPs in such a Josephson junction is the subharmonic gap structure (SGS); a series of resonant conductance peaks in a voltage-biased Josephson junction resulting from multiple Andreev reflections (MAR) [24]. In conventional Josephson junctions, the SGS peaks appear at $eV_n = 2\Delta_0/n$, with Δ_0 the superconducting gap and n an integer number [25–30]. By contrast, due to the presence of MBSs in topological Josephson junctions, new resonant channels form in the middle of the energy gap leading to an anomalous SGS with only even integer peaks. That is, the conductance resonances are located at $eV_m = 2\Delta_0/m$ where m is now an even integer [31–33]. Anomalous SGSs have been predicted in Josephson junctions mediated by the edge states of a QSHI, which were interpreted as a parity-changing process in a topological Josephson junction [31]. Angle-resolved SGS have

also been explored in two-dimensional Josephson junctions for detecting chiral Majorana states [34]. However, such setups require breaking time-reversal symmetry by Zeeman coupling at the QSHI edges, thus hindering their experimental implementation.

In this paper we consider time-reversal invariant QSHI strips where two opposite edges are covered by superconductors with a tunable phase difference. We consider normal-metal (N)/insulator (I)/S [Fig. 1(a)] and S/I/S [Fig. 1(b)] junctions where the edge states of the two sides of the strip are not disconnected. Consequently, the edge states hybridize and their characteristic Dirac-like linear dispersion becomes gapped by 2α , with α the coupling strength. We further assume that the chemical potential for the insulating region ($0 < x < L$) is tuned to the middle of the gap, but remains large ($\mu \gg \alpha$) for the N ($x < 0$) and S ($x > L$) regions, thus forming a tunnel junction of variable transmission. A bias voltage at terminals 1 and 2 injects a current which is collected by terminals 3 and 4 at the S side, see Fig. 1. The phase difference ϕ between superconductors can be controlled by a magnetic flux. For $\phi = \pi$ the system preserves time-reversal symmetry and can host MKPs. As a result, the zero-bias N/I/S conductance is quantized to $4e^2/h$.

Interestingly, the SGS for the S/I/S junction can be tuned by ϕ in clear contrast with conventional Josephson junctions. For $\phi = 0$, the SGS features peaks at $eV_m = 2\Delta_{L/R}/m$ and $eV_n = (\Delta_L + \Delta_R)/n$, with m and n being, respectively, even and odd integers, and Δ_L (Δ_R) the left (right) pair potential. Moreover, for asymmetric junctions ($\Delta_L \neq \Delta_R$) only the even spikes of the SGS split. These results are in good agreement with the behavior of conventional BCS Josephson junctions [35]. By contrast, in the topological phase with $\phi = \pi$, featuring time-reversal invariant MKPs, only the even resonant peaks ($eV_m = 2\Delta_{L/R}/m$) appear, and all spikes split for asymmetric junctions. We further show that the necessary condition for observing resonant spikes in the SGS in the topological phase is the enhanced amplitude of the multiple Andreev reflection via midgap bound

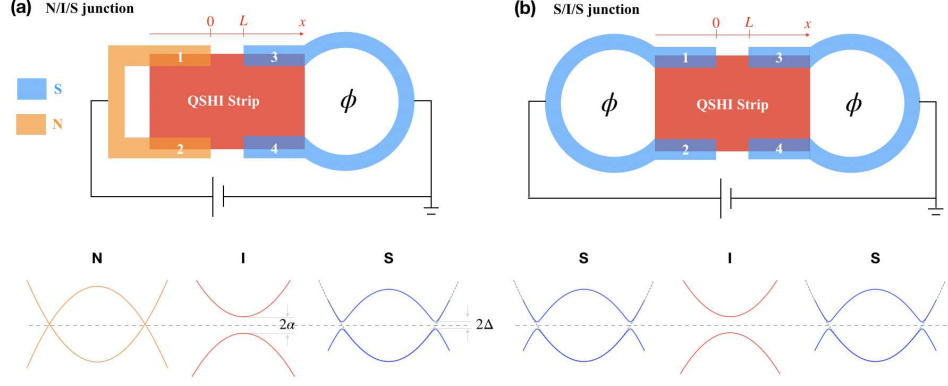


FIG. 1. Schematic diagram of the device layout to detect a topological transition: (a) N/I/S and (b) S/I/S junctions. The superconducting phase difference between terminals is controlled by a magnetic flux. Terminals 1 and 2 connect to a normal injection electrode in (a) and to a superconducting one in (b). Terminals 3 and 4 connect to the right superconducting electrode. Schematic band structures of low-energy quasiparticles in each region are shown below the devices.

states. While, for non-topological states, both even- and odd-order MAR give rise to SGS originating from the divergent density of states at the trivial gap edges.

The rest of the paper is organized as follows. In Section II, we describe the model. We present the transport properties of N/I/S and S/I/S junctions in Sections III and IV, respectively. Finally, we conclude this work with a brief summary in Section V.

II. MODEL AND FORMALISM.

The low-energy effective edge state Hamiltonian is given by $\mathcal{H} = \mathcal{H}_0 + \mathcal{H}_S$ with

$$\mathcal{H}_0 = \int dx \hat{\Psi}^\dagger [-i\hbar v \hat{\sigma}_z \hat{s}_z \partial_x + \alpha \hat{\sigma}_x - \mu] \hat{\Psi}, \quad (1)$$

$$\mathcal{H}_S = \Delta \int dx \left[\hat{\Psi}_{1,\uparrow}^\dagger \hat{\Psi}_{1,\downarrow}^\dagger + e^{i\phi} \hat{\Psi}_{-1,\uparrow}^\dagger \hat{\Psi}_{-1,\downarrow}^\dagger \right] + \text{h.c.}, \quad (2)$$

and basis $\hat{\Psi} = (\hat{\Psi}_{1,\uparrow}^\dagger, \hat{\Psi}_{1,\downarrow}^\dagger, \hat{\Psi}_{-1,\uparrow}^\dagger, \hat{\Psi}_{-1,\downarrow}^\dagger)^T$. Here, the subscript $\sigma \in \{1, -1\}$ labels the different edges and the Pauli matrices $\hat{\sigma}_i$ and \hat{s}_i , with $i \in \{x, y, z\}$, act on edge and spin spaces, respectively. The chemical potential is $\mu(x) = \mu [\Theta(-x) + \Theta(x-L)]$, with $\Theta(x)$ being the Heaviside step function and L the junction length, and α is the coupling strength between opposite edges [36]. We define the pair potential $\Delta(x) = \Delta_0 \Theta(x-L)$ for the N/I/S junction [Fig. 1(a)] and $\Delta(x) = \Delta_L \Theta(-x) + \Delta_R \Theta(x-L)$ for the S/I/S junction [Fig. 1(b)]. Using the Bogoliubov transformation $\hat{\Psi}_{\sigma,s} = \sum_N u_{\sigma,s}^N \hat{\gamma}_N + v_{\sigma,s}^{N,*} \hat{\gamma}_N^\dagger$, we derive the Bogoliubov-de Gennes (BdG) Hamiltonian $H = H_1 \oplus H_2$, with

$$H_{\eta=1,2} = \begin{pmatrix} \hat{h}_\eta & \hat{\Delta}_\eta \\ \hat{\Delta}_\eta^\dagger & -\hat{h}_\eta \end{pmatrix}, \quad (3)$$

and

$$\hat{h}_{1(2)} = \begin{pmatrix} \mp i\hbar v \partial_x - \mu & \alpha \\ \alpha & \pm i\hbar v \partial_x - \mu \end{pmatrix}, \quad (4)$$

$$\hat{\Delta}_{1(2)} = \begin{pmatrix} \pm \Delta & 0 \\ 0 & \pm \Delta e^{i\phi} \end{pmatrix}, \quad (5)$$

where H_1 (H_2) acts on $(u_{1,\uparrow}^N, u_{-1,\uparrow}^N, v_{1,\downarrow}^N, v_{-1,\downarrow}^N)^T$ [$(u_{1,\downarrow}^N, u_{-1,\downarrow}^N, v_{1,\uparrow}^N, v_{-1,\uparrow}^N)^T$] space. The wavefunctions can be found in Appendix A.

For the N/I/S junction, the wavefunction for an incident electron from the N side is

$$\Phi = \sum_{\eta=1,2} \left[\psi_{\eta,N}^{e,\rightarrow} + b_\eta \psi_{\eta,N}^{e,\leftarrow} + a_\eta \psi_{\eta,N}^{h,\leftarrow} \right]. \quad (6)$$

The conductance can be obtained as [37]

$$G = G_0 \sum_\eta \left[1 - |b_\eta|^2 + |a_\eta|^2 \right], \quad (7)$$

with $G_0 = e^2/h$ being the conductance quantum.

For the S/I/S junction, the time-dependent wavefunctions at the central scattering region, $(0, L)$, for an incident quasiparticle from terminal 1 read

$$\Phi_{x=0^-} = \sum_n e^{-i \frac{(\epsilon + 2n e V)t}{\hbar}} \begin{pmatrix} (J_\epsilon^{(1)} \delta_{n,0} + a_{L,2n} A_n) \\ B_n \\ A_n \\ a_{L,2n} e^{-i\phi} B_n \end{pmatrix}, \quad (8)$$

$$\Phi_{x=L^+} = \sum_n e^{-i \frac{[\epsilon + (2n+1)eV]t}{\hbar}} \begin{pmatrix} C_n \\ a_{R,2n+1} e^{i\phi} D_n \\ a_{R,2n+1} C_n \\ D_n \end{pmatrix}, \quad (9)$$

where $a_{L/R,n} \equiv a_{L/R}(\epsilon + n e V)$ with

$$a_{L/R}(\epsilon) = \begin{cases} \frac{\epsilon - \text{sgn}(\epsilon) (\epsilon^2 - \Delta_{L/R}^2)^{1/2}}{\Delta_{L/R}}, & |\epsilon| > \Delta_{L/R} \\ \frac{\epsilon - i (\Delta_{L/R}^2 - \epsilon^2)^{1/2}}{\Delta_{L/R}}, & |\epsilon| < \Delta_{L/R}. \end{cases}, \quad (10)$$

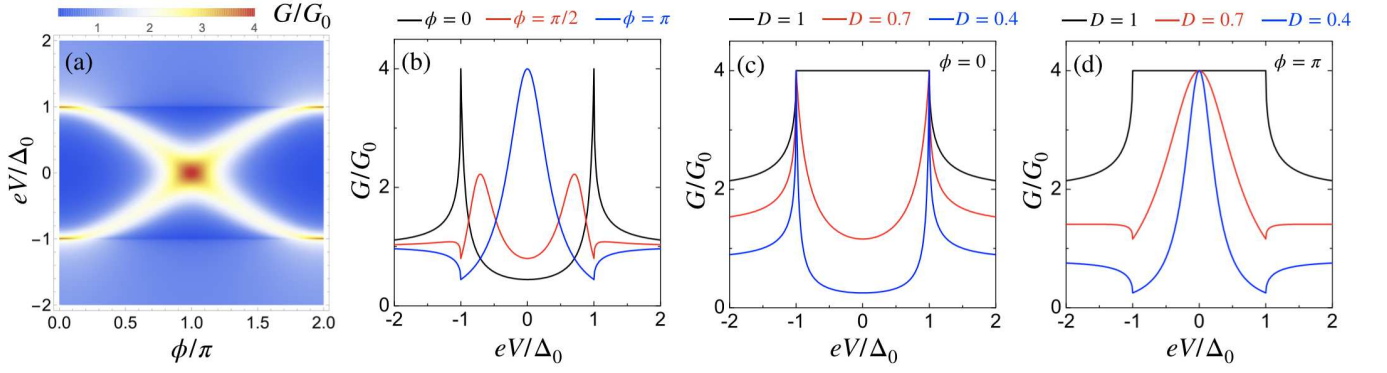


FIG. 2. N/I/S junction: (a) Contour plot of the conductance G/G_0 , with $G_0 = e^2/h$, as a function of the phase ϕ and bias voltage eV . The transmissivity is $D = 0.5$. Conductance in (a) vs bias voltage for different phase differences $\phi = 0$ (black), $\pi/2$ (red), and π (blue). (c) Conductance with the phase $\phi = 0$ for $D = 1$ (black), 0.7 (red) and 0.5 (blue). (d) Same as (c) for $\phi = \pi$.

and $J_\epsilon^{(1)} = \sqrt{1 - |a_L(\epsilon)|^2}$ being the amplitude of the incident quasiparticle from terminal 1 into the scattering region. The wavefunctions Φ_{0-} and Φ_{L+} are connected by the scattering matrices

$$S_e = S_h^* = \begin{bmatrix} r & t \\ t & -r^*t/t^* \end{bmatrix}, \quad (11)$$

with $r = -i \tanh(\alpha L/v)$, $t = 1/\cosh(\alpha L/v)$. Here, we have assumed that $\alpha \gg \Delta_{L/R}$ and thus the scattering

matrices can be approximated as energy independent. Consequently, the coefficients A_n , B_n , C_n , and D_n are related by

$$\begin{pmatrix} B_n \\ C_n \end{pmatrix} = S_e \begin{pmatrix} J_\epsilon^{(1)} \delta_{n,0} + a_{L,2n} A_n \\ a_{R,2n+1} e^{i\phi} D_n \end{pmatrix}, \quad (12)$$

$$\begin{pmatrix} A_n \\ D_{n-1} \end{pmatrix} = S_h \begin{pmatrix} a_{L,2n} e^{-i\phi} B_n \\ a_{R,2n-1} C_{n-1} \end{pmatrix}. \quad (13)$$

Solving Eqs. (12) and (13), we obtain the following recurrence relations for A_n and B_n

$$A_{1,n+1} - a_{R,2n+1} a_{L,2n} A_{1,n} = |r| a_{L,2n+2} e^{-i\phi} B_{1,n+1} - |r| a_{R,2n+1} B_{1,n} + a_{R,1} J_\epsilon^{(1)} \delta_{n,0}, \quad (14)$$

$$\begin{aligned} \frac{D a_{L,2n+2} a_{R,2n+1}}{1 - a_{R,2n+1}^2 e^{i\phi}} B_{1,n+1} - \left[\frac{D a_{R,2n+1}^2 e^{i\phi}}{1 - a_{R,2n+1}^2 e^{i\phi}} + \frac{D a_{L,2n}^2 e^{-i\phi}}{1 - a_{R,2n-1}^2 e^{i\phi}} - e^{-i\phi} a_{L,2n}^2 + 1 \right] B_{1,n} + \frac{D a_{R,2n-1} a_{L,2n}}{1 - a_{R,2n-1}^2 e^{i\phi}} B_{1,n-1} \\ = -|r| J_\epsilon^{(1)} \delta_{n,0}, \end{aligned} \quad (15)$$

Next, from the continuity equation $\frac{\partial}{\partial t} \hat{\rho} + \partial_x \hat{\mathcal{J}} = 0$, with $\hat{\rho} = e \sum_\sigma (\Psi_{\sigma,\uparrow}^\dagger \Psi_{\sigma,\uparrow} + \Psi_{\sigma,\downarrow}^\dagger \Psi_{\sigma,\downarrow})$, we define the current operator $\hat{\mathcal{J}} = \sum_\sigma \frac{ev\sigma}{\hbar} (\Psi_{\sigma,\uparrow}^\dagger \Psi_{\sigma,\uparrow} - \Psi_{\sigma,\downarrow}^\dagger \Psi_{\sigma,\downarrow})$. The average electric current in terminal 1, cf. Eq. (8), is defined as

$$\begin{aligned} I_1 = \langle \hat{\mathcal{J}} \rangle = \frac{e}{\hbar} \sum_{k,n} e^{i \frac{2keVt}{\hbar}} \int_{-\infty}^{+\infty} d\epsilon \left[\left(J_\epsilon^{(1)} \delta_{n+k,0} + a_{L,2(n+k)}^* A_{1,n+k}^* \right) \left(J_\epsilon^{(1)} \delta_{n,0} + a_{L,2n} A_{1,n} \right) - B_{1,n+k}^* B_{1,n} \right] f_\epsilon \\ + \frac{e}{\hbar} \sum_{k,n} e^{i \frac{2keVt}{\hbar}} \int_{-\infty}^{+\infty} d\epsilon \left[a_{L,2n} a_{L,2(n+k)}^* B_{1,n+k}^* B_{1,n} - A_{1,n+k}^* A_{1,n} \right] f_{-\epsilon}, \end{aligned} \quad (16)$$

where $f_\epsilon = (e^{\epsilon/k_B T} + 1)^{-1}$ is the Fermi-Dirac distribution function. The dc component of the current corresponds to the $k = 0$ harmonic in Eq. (16). Similarly, we can obtain the currents for the other terminals, $I_{i=2-4}$, and obtain the total current as $I = \sum_i I_i$ (see Appendix B). In the numerical calculations, we solved Eq. (15) by choos-

ing an appropriate cut-off value $|n| = N$, and normalize it in units of $G_N \Delta/e$, where G_N is the conductance when all electrodes are in the normal state. The differential conductance is thus obtained as $G = \partial I / \partial V$.

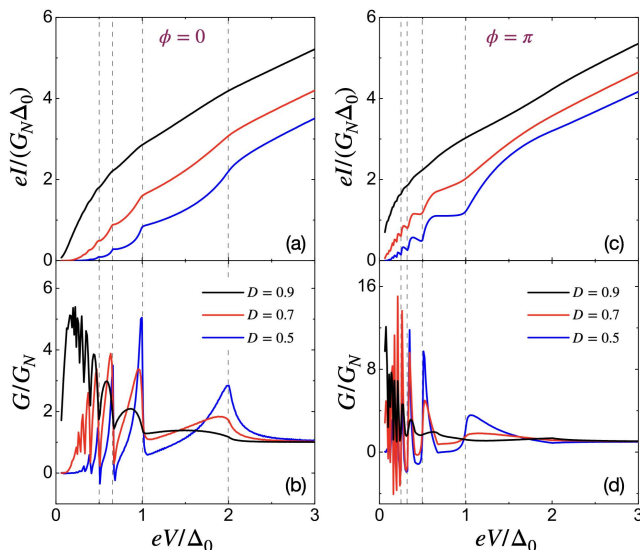


FIG. 3. S/I/S junction: Electric current and differential conductance at temperature $k_B T = 0.2\Delta_0$ as a function of the voltage, for $\phi = 0$ (a,b) and $\phi = \pi$ (c,d), for transmissions $D = 0.9, 0.7, 0.5$. In all cases, $\Delta_L = \Delta_R = \Delta_0$. The dashed vertical lines indicate the positions of the resonant spikes.

III. TUNNELING SPECTROSCOPY OF N/I/S JUNCTIONS

The emergence of a time-reversal invariant topological superconductor becomes apparent in the tunneling spectroscopy. Thus, we first calculate the differential conductance dI/dV using Eq. (7). The conductance spectra as a function of phase difference ϕ and the bias voltage eV is shown in Fig. 2(a), with transmissivity $D = tt^* = 0.5$. The subgap resonance peaks vary with ϕ and cross at $\phi = \pi$, where the topological phase transition takes place. For $\phi = 0$, the conductance reaches the value $G = 4e^2/h$ at $eV = \pm\Delta_0$, see Fig. 2(b), which indicates a perfect Andreev reflection at the gap edges [38]. Indeed, the conductance for $\phi = 0$ behaves like an s -wave superconductor where the subgap values reduce by decreasing transmissivity D [37] [Fig. 2(c)]. As expected, these quantized peaks merge at $eV = 0$ for $\phi = \pi$ where the MKPs appear, i.e., a single Majorana bound state contributes $2e^2/h$ to the conductance. Moreover, the conductance quantization remains robust against D for $\phi = \pi$, exhibiting the celebrated zero-biased conductance peak due to Majorana states [39–56] [Fig. 2(d)]. At the same time, the π -difference decreases the local density of states at the gap edges $eV = \pm\Delta_0$.

IV. MULTIPLE ANDREEV REFLECTIONS IN S/I/S JUNCTIONS

We now calculate the current at the S/I/S junction, see Fig. 3. We focus on the dc current which experimen-

tally relates to the average electric current in the long time limit. Our formalism can be applied to arbitrary value of ϕ , but, for clarity, we focus on the time-reversal invariant junction with $\phi = 0$ and $\phi = \pi$. In Fig. 3, we consider a symmetric junction with $\Delta_L = \Delta_R = \Delta_0$, and show the current and differential conductance for different values of the transmission. For $\phi = 0$, the current characteristic is that of s -wave superconductors, where the conductance displays peaks at $eV_n = 2\Delta_0/n$ (n being an integer), see Fig. 3(a,b). By contrast, the SGS becomes $2\Delta_0/m$ (m an even integer) for $\phi = \pi$, see Fig. 3(c,d). A SGS with only even resonances was already predicted for time-reversal breaking topological Josephson junctions with zero-energy states [31–33]. The exotic SGS can be understood as follows. In the topological superconducting phase, the density of states at the gap edges is suppressed, in contrast to the divergent density for trivial superconductors, cf. the N/I/S conductance spectra in Fig. 2. Thus, MAR processes where

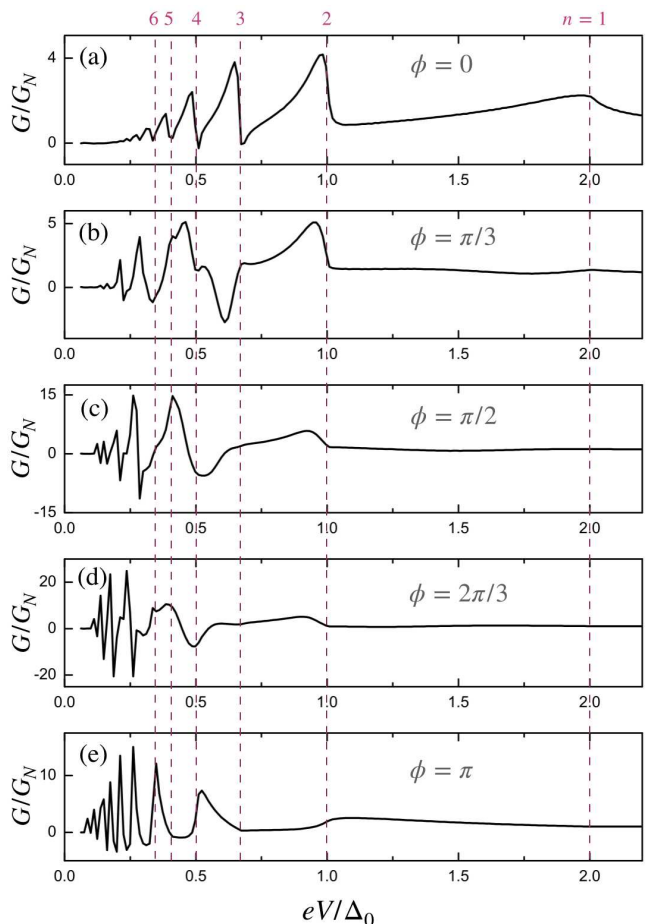


FIG. 4. Differential conductance as a function of the voltage at temperature $k_B T = 0.2\Delta_0$ for (a) $\phi = 0$, (b) $\phi = \pi/3$, (c) $\phi = \pi/2$, (d) $\phi = 2\pi/3$, and (e) $\phi = \pi$. The dashed vertical lines mark the n -th order SGS at $2\Delta_0/n$ for $n = 1, 2, 3, 4, 5, 6$. In all cases, we choose $\Delta_L = \Delta_R = \Delta_0$ and $D = 0.6$.

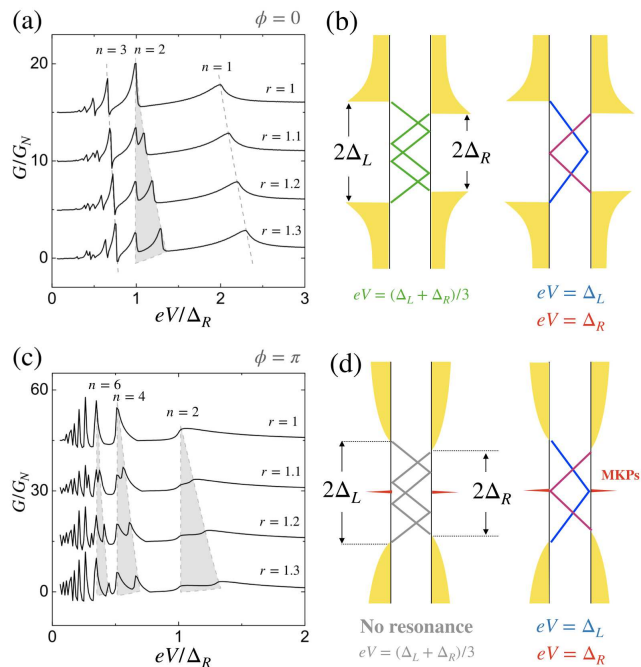


FIG. 5. Differential conductance at temperature $k_B T = 0.2\Delta_0$ for $D = 0.6$ as the gap ratio $r = \Delta_L/\Delta_R$ varies for (a) $\phi = 0$ and (c) $\phi = \pi$. (b) and (d) show the schematic trajectories of the third-order and the second-order MAR.

quasiparticles transmit from the lower gap edge at $-\Delta_0$ to the upper one at Δ_0 will not necessarily give rise to conductance peaks. By contrast, when the MAR trajectory passes through the midgap MBSs, the resonant channel will boost the MAR transmission and therefore a conductance peak appears. Consequently, the presence of zero-energy states (now MKPs) when $\phi = \pi$ plays an important role in forming the SGS. It is also interesting to compare our results with previous works on phase-tuned MAR in multi-terminal superconductors [57–60]. In a conventional 3-terminal s -wave superconducting interferometer, the phase difference changes the visibility, instead of the shape of the SGS. However, in our setup, the phase difference directly changes the characteristic of the SGS.

To further show how the SGSs evolve with the phase difference, we plot the conductance spectra with equal pair potential $\Delta_L = \Delta_R = \Delta_0$ in Fig. 4. Apart from the previously analyzed cases with $\phi = 0$ and π , the position of the resonant peaks in the SGS is not straightforward to identify. However, it is clear that the odd order resonances gradually disappear by increasing ϕ from 0 to π . Thus, as the phase reaches $\phi = \pi$, only the even order resonant peaks remain in the SGS.

Next, we explore the SGS in asymmetric junctions where Δ_L and Δ_R can be different. We focus on the time reversal invariant cases $\phi = 0, \pi$ and compare them to the symmetric case. In Fig. 5(a), we consider a trivial junc-

tion with $\phi = 0$ and change the gap ratio $r = \Delta_L/\Delta_R$. For $\Delta_L \neq \Delta_R$, the odd order resonant conductance peaks remain at $eV_n = (\Delta_L + \Delta_R)/n$ (n odd), while the even order ones at $eV_m = 2\Delta_{L/R}/m$ (m even) split into two, see shaded area in Fig. 5(a). To illustrate this difference, we sketch the second and third order MAR processes in Fig. 5(b). Since the SGS appears when MAR connect with two band edges, for odd integers (green lines) quasiparticles climb up the same energy $\Delta_L + \Delta_R$ via MAR. Thus the SGS for $eV_3 = (\Delta_L + \Delta_R)/3$ does not split. For even order MAR, however, the two possible paths for quasiparticles gain different energy as indicated by the blue and red lines. Therefore, the second order MAR contribute double peaks at $eV_n = \Delta_L$ and $eV_n = \Delta_R$ to the conductance spectra.

Next, we consider the nontrivial case with $\phi = \pi$ and keep the other parameters unchanged. As for symmetric junctions, the odd order MAR resonances disappear [Fig. 5(c)] due to the reduced density of states at the gap edges. As explained above, MAR processes connecting two gap edges only give rise to SGS when a zero-energy state resides in its trajectory. It explains why the odd order gray MAR trajectories sketched in Fig. 5(d) do not contribute to SGS. However, the even order blue and red MAR processes satisfy the resonant condition and thus enhance the onset current leading to the appearance of conductance peaks. This analysis of the SGS is also valid for time-reversal broken topological superconductors.

V. CONCLUSIONS

We have studied the charge transport properties of quantum spin Hall strips with coupled edge states, connected to several normal and superconducting electrodes. The current characteristics strongly change with the superconducting phase difference between the opposite edges. We find quantized conductance peaks in the normal metal/insulator/superconductor junction as a signature of time-reversal invariant Kramers pairs of Majoranas. We also find that the subharmonic gap structure is very sensitive to the phase difference. In the topological phase with $\phi = \pi$, the odd order multiple Andreev processes do not contribute to the current, and only the even order ones appear in the subharmonic gap structure due to the presence of zero-energy Majorana states. Our proposal for the observation of time-reversal invariant Kramers pairs of Majoranas is within experimental reach, after recent advances implementing superconducting electrodes on semiconductor quantum wells [61–65].

Acknowledgment. We thank Yukio Tanaka and Fanning Qu for valuable discussions. B. L. acknowledges support from the National Natural Science Foundation of China (project 11904257) and the Natural Science Foundation of Tianjin (project 20JCQNJC01310). P. B. acknowledges support from the Spanish CM ‘‘Talento Program’’ Project no. 2019-T1/IND-14088 and the Spanish Ministerio de Ciencia e Innovaci3n Grant no. PID2020-117992GA-I00.

Appendix A: Wavefunctions

In the superconducting side, we can transform the Hamiltonian using the unitary transformation

$$U = \frac{1}{\sqrt{2}} \begin{bmatrix} 1 & 1 & 0 & 0 \\ 1 & -1 & 0 & 0 \\ 0 & 0 & -1 & -1 \\ 0 & 0 & -1 & 1 \end{bmatrix}, \quad (\text{A.1})$$

and $\tilde{H}_{1(2)} = UH_{1(2)}U^\dagger$ becomes

$$\tilde{H}_{1(2)} = \begin{bmatrix} -\mu + \alpha & \mp i\partial_x & \mp \gamma\xi_c\Delta & \mp i\gamma\xi_s\Delta \\ \mp i\partial_x & -\mu - \alpha & \pm i\gamma\xi_s\Delta & \pm \gamma\xi_c\Delta \\ \mp \gamma^*\xi_c\Delta & \mp i\gamma^*\xi_s\Delta & \mu - \alpha & \mp i\partial_x \\ \pm i\gamma^*\xi_s\Delta & \pm \gamma^*\xi_c\Delta & \mp i\partial_x & \mu + \alpha \end{bmatrix}, \quad (\text{A.2})$$

with $\xi_c = \cos \frac{\phi}{2}$, $\xi_s = \sin \frac{\phi}{2}$, and $\gamma = e^{i\frac{\phi}{2}}$. It can be seen that α is negligible in $\tilde{H}_{1(2)}$ in the limit $\alpha \ll \mu$, and if $\phi \neq 0$ or π there are mixed singlet- and triplet-pairings. The wavefunction ψ of $H_{1(2)}$ can be obtained by $U^\dagger\tilde{\psi}$, where $\tilde{\psi}$ is the solution of $\tilde{H}_{1(2)}$. The wavefunctions of H_1 in the superconducting side are

$$\psi_{1,S}^{e,\rightarrow} = [u, 0, v, 0]^T e^{ikx}, \quad (\text{A.3})$$

$$\psi_{1,S}^{e,\leftarrow} = [0, u, 0, ve^{-i\phi}]^T e^{-ikx}, \quad (\text{A.4})$$

$$\psi_{1,S}^{h,\rightarrow} = [0, ve^{i\phi}, 0, u]^T e^{-ikx}, \quad (\text{A.5})$$

$$\psi_{1,S}^{h,\leftarrow} = [v, 0, u, 0]^T e^{ikx}, \quad (\text{A.6})$$

and the wavefunctions of H_2 in the superconducting side are

$$\psi_{2,S}^{e,\rightarrow} = [0, u, 0, -ve^{-i\phi}]^T e^{ikx}, \quad (\text{A.7})$$

$$\psi_{2,S}^{e,\leftarrow} = [u, 0, -v, 0]^T e^{-ikx}, \quad (\text{A.8})$$

$$\psi_{2,S}^{h,\rightarrow} = [-v, 0, u, 0]^T e^{-ikx}, \quad (\text{A.9})$$

$$\psi_{2,S}^{h,\leftarrow} = [0, -ve^{i\phi}, 0, u]^T e^{ikx}, \quad (\text{A.10})$$

where u and v are the coherent factors

$$u(\epsilon) = \sqrt{\frac{1}{2} \left(1 + \frac{\sqrt{\epsilon^2 - \Delta^2}}{\epsilon} \right)}, \quad (\text{A.11})$$

$$v(\epsilon) = \sqrt{\frac{1}{2} \left(1 - \frac{\sqrt{\epsilon^2 - \Delta^2}}{\epsilon} \right)}. \quad (\text{A.12})$$

In the central scattering region $0 < x < L$, the wavefunctions are given by

$$\psi_{1,c}^{e,1} = [i, 1, 0, 0]^T e^{-\kappa x}, \quad (\text{A.13})$$

$$\psi_{1,c}^{e,2} = [-i, 1, 0, 0]^T e^{\kappa x}, \quad (\text{A.14})$$

$$\psi_{1,c}^{h,1} = [0, 0, i, 1]^T e^{-\kappa x}, \quad (\text{A.15})$$

$$\psi_{1,c}^{h,2} = [0, 0, -i, 1]^T e^{\kappa x}, \quad (\text{A.16})$$

and

$$\psi_{2,c}^{e,1} = [-i, 1, 0, 0]^T e^{-\kappa x}, \quad (\text{A.17})$$

$$\psi_{2,c}^{e,2} = [i, 1, 0, 0]^T e^{\kappa x}, \quad (\text{A.18})$$

$$\psi_{2,c}^{h,1} = [0, 0, -i, 1]^T e^{-\kappa x}, \quad (\text{A.19})$$

$$\psi_{2,c}^{h,2} = [0, 0, i, 1]^T e^{\kappa x}, \quad (\text{A.20})$$

with $\kappa = \alpha/v$.

Appendix B: Recursive relations and currents in the S/I/S junction

In the main text, we have derived the current from injected quasiparticles in terminal 1. We now provide the calculation of currents induced by injection from the other three terminals. The recursive equations for a quasiparticle incident from terminal 2 are

$$A_{2,n+1} - a_{R,2n+1}a_{L,2n}A_{2,n} = |r|a_{L,2n+2}e^{i\phi}B_{2,n+1} - |r|a_{R,2n+1}B_{2,n} + a_{R,1}J_\epsilon^{(2)}\delta_{n0}, \quad (\text{B.1})$$

$$\begin{aligned} \frac{Da_{L,2n+2}a_{R,2n+1}}{1 - \bar{a}_{R,2n+1}^2 e^{-i\phi}} B_{2,n+1} - \left[\frac{Da_{R,2n+1}^2 e^{-i\phi}}{1 - \bar{a}_{R,2n+1}^2 e^{-i\phi}} + \frac{Da_{L,2n}^2 e^{i\phi}}{1 - \bar{a}_{R,2n-1}^2 e^{-i\phi}} - e^{i\phi} \bar{a}_{L,2n}^2 + 1 \right] B_{2,n} + \frac{Da_{R,2n-1}a_{L,2n}}{1 - \bar{a}_{R,2n-1}^2 e^{-i\phi}} B_{2,n-1} \\ = -|r|J_\epsilon^{(2)}\delta_{n0}. \end{aligned} \quad (\text{B.2})$$

For an incident quasiparticle from terminal 3, the relations are

$$\bar{A}_{3,n+1} - \bar{a}_{L,2n+1}\bar{a}_{R,2n}\bar{A}_{3,n} = |r|\bar{a}_{R,2n+2}e^{i\phi}\bar{B}_{3,n+1} - |r|\bar{a}_{L,2n+1}\bar{B}_{3,n} + \bar{a}_{L,1}J_\epsilon^{(3)}\delta_{n0}, \quad (\text{B.3})$$

$$\begin{aligned} \frac{D\bar{a}_{L,2n+1}\bar{a}_{R,2n+2}}{1 - \bar{a}_{L,2n+1}^2 e^{-i\phi}} \bar{B}_{3,n+1} - \left[\frac{D\bar{a}_{L,2n+1}e^{-i\phi}}{1 - \bar{a}_{L,2n+1}^2 e^{-i\phi}} + \frac{D\bar{a}_{R,2n}e^{i\phi}}{1 - \bar{a}_{L,2n-1}^2 e^{-i\phi}} - e^{i\phi}\bar{a}_{R,2n}^2 + 1 \right] \bar{B}_{3,n} + \frac{D\bar{a}_{L,2n-1}\bar{a}_{R,2n}}{1 - \bar{a}_{L,2n-1}^2 e^{-i\phi}} \bar{B}_{3,n-1} \\ = -|r|J_\epsilon^{(3)}\delta_{n0}. \end{aligned} \quad (\text{B.4})$$

And for terminal 4, they are

$$\bar{A}_{4,n+1} - \bar{a}_{L,2n+1}\bar{a}_{R,2n}\bar{A}_{4,n} = |r|\bar{a}_{R,2n+2}e^{-i\phi}\bar{B}_{4,n+1} - |r|\bar{a}_{L,2n+1}\bar{B}_{4,n} + \bar{a}_{L,1}J_\epsilon^{(4)}\delta_{n0}, \quad (\text{B.5})$$

$$\begin{aligned} \frac{D\bar{a}_{L,2n+1}\bar{a}_{R,2n+2}}{1 - \bar{a}_{L,2n+1}e^{i\phi}} \bar{B}_{4,n+1} - \left[\frac{D\bar{a}_{L,2n+1}e^{i\phi}}{1 - \bar{a}_{L,2n+1}^2 e^{i\phi}} + \frac{D\bar{a}_{R,2n}^2 e^{-i\phi}}{1 - \bar{a}_{L,2n-1}^2 e^{i\phi}} - e^{-i\phi}\bar{a}_{R,2n}^2 + 1 \right] \bar{B}_{4,n} + \frac{D\bar{a}_{L,2n-1}\bar{a}_{R,2n}}{1 - \bar{a}_{L,2n-1}^2 e^{i\phi}} \bar{B}_{4,n-1} \\ = -|r|J_\epsilon^{(4)}\delta_{n0}. \end{aligned} \quad (\text{B.6})$$

Here, \bar{a} is defined as $\bar{a}_{L/R,n} = a_{L/R}(\epsilon - neV)$. The current sources $J_\epsilon^{(i)}$ are given by $J_\epsilon^{(2)} = \sqrt{1 - |a_L(\epsilon)|^2}$ and $J_\epsilon^{(3)} = J_\epsilon^{(4)} = \sqrt{1 - |a_R(\epsilon)|^2}$. We have defined $A_n = A(n, eV)$, $B_n = B(n, eV)$, $\bar{A}_n = A(n, -eV)$ and $\bar{B}_n = B(n, -eV)$. The resulting currents I_2 , I_3 , and I_4 are derived as

$$\begin{aligned} I_2 = \frac{e}{h} \sum_k e^{i\frac{2k\epsilon V t}{h}} \int_{-\infty}^{+\infty} d\epsilon \sum_n \left[\left(J_\epsilon^{(2)} \delta_{n+k,0} + a_{L,2(n+k)}^* A_{2,n+k}^* \right) \left(J_\epsilon^{(2)} \delta_{n,0} + a_{L,2n} A_{2,n} \right) - B_{2,n+k}^* B_{2,n} \right] f_\epsilon \\ + \frac{e}{h} \sum_k e^{i\frac{2k\epsilon V t}{h}} \int_{-\infty}^{+\infty} d\epsilon \sum_n \left[a_{L,2n} a_{L,2(n+k)}^* B_{2,n+k}^* B_{2,n} - A_{2,n+k}^* A_{2,n} \right] f_{-\epsilon}, \end{aligned} \quad (\text{B.7})$$

$$\begin{aligned} I_3 = \frac{e}{h} \sum_k e^{i\frac{2k\epsilon V t}{h}} \int_{-\infty}^{+\infty} d\epsilon \sum_n \left[- \left(J_\epsilon^{(3)} \delta_{n+k,0} + \bar{a}_{R,2(n+k)}^* \bar{A}_{3,n+k}^* \right) \left(J_\epsilon^{(3)} \delta_{n,0} + \bar{a}_{R,2n} \bar{A}_{3,n} \right) + \bar{B}_{3,n+k}^* \bar{B}_{3,n} \right] f_\epsilon \\ + \frac{e}{h} \sum_k e^{i\frac{2k\epsilon V t}{h}} \int_{-\infty}^{+\infty} d\epsilon \sum_n \left[-\bar{a}_{R,2n} a_{R,2(n+k)}^* \bar{B}_{3,n+k}^* \bar{B}_{3,n} + \bar{A}_{3,n+k}^* \bar{A}_{3,n} \right] f_{-\epsilon}, \end{aligned} \quad (\text{B.8})$$

$$\begin{aligned} I_4 = \frac{e}{h} \sum_k e^{i\frac{2k\epsilon V t}{h}} \int_{-\infty}^{+\infty} d\epsilon \sum_n \left[- \left(J_\epsilon^{(4)} \delta_{n+k,0} + \bar{a}_{R,2(n+k)}^* \bar{A}_{4,n+k}^* \right) \left(J_\epsilon^{(4)} \delta_{n,0} + \bar{a}_{R,2n} \bar{A}_{4,n} \right) + \bar{B}_{4,n+k}^* \bar{B}_{4,n} \right] f_\epsilon \\ + \frac{e}{h} \sum_k e^{i\frac{2k\epsilon V t}{h}} \int_{-\infty}^{+\infty} d\epsilon \sum_n \left[-\bar{a}_{R,2n} a_{R,2(n+k)}^* \bar{B}_{4,n+k}^* \bar{B}_{4,n} + \bar{A}_{4,n+k}^* \bar{A}_{4,n} \right] f_{-\epsilon}. \end{aligned} \quad (\text{B.9})$$

[1] C. L. Kane and E. J. Mele, Quantum spin hall effect in graphene, *Phys. Rev. Lett.* **95**, 226801 (2005).

[2] C. L. Kane and E. J. Mele, Z_2 topological order and the quantum spin hall effect, *Phys. Rev. Lett.* **95**, 146802

- (2005).
- [3] B. A. Bernevig, T. L. Hughes, and S. C. Zhang, Quantum spin Hall effect and topological phase transition in HgTe quantum wells, *Science* **314**, 1757 (2006).
 - [4] C. Liu, T. L. Hughes, X.-L. Qi, K. Wang, and S.-C. Zhang, Quantum spin Hall effect in inverted type-II semiconductors, *Phys. Rev. Lett.* **100**, 236601 (2008).
 - [5] C. Wu, B. A. Bernevig, and S.-C. Zhang, Helical Liquid and the Edge of Quantum Spin Hall Systems, *Phys. Rev. Lett.* **96**, 106401 (2006).
 - [6] C. Xu and J. E. Moore, Stability of the quantum spin hall effect: Effects of interactions, disorder, and F_2 topology, *Phys. Rev. B* **73**, 045322 (2006).
 - [7] A. Roth, C. Brüne, H. Buhmann, L. W. Molenkamp, J. Maciejko, X.-L. Qi, and S.-C. Zhang, Nonlocal Transport in the Quantum Spin Hall State, *Science* **325**, 294 (2010).
 - [8] C. Brüne, A. Roth, H. Buhmann, E. M. Hankiewicz, L. W. Molenkamp, J. Maciejko, X.-L. Qi, and S.-C. Zhang, Spin polarization of the quantum spin Hall edge states, *Nat. Phys.* **8**, 485 (2012).
 - [9] C.-H. Hsu, P. Stano, J. Klinovaja, and D. Loss, Helical liquids in semiconductors, *Semicond. Sci. Tech.* **36**, 123003 (2021).
 - [10] A. Kitaev, Unpaired majorana fermions in quantum wires, *PHYS-USP+* **44**, 131 (2001).
 - [11] A. Kitaev, Fault-tolerant quantum computation by anyons, *Ann Phys (N Y)* **303**, 2 (2003).
 - [12] C. Nayak, S. H. Simon, A. Stern, M. Freedman, and S. Das Sarma, Non-abelian anyons and topological quantum computation, *Rev. Mod. Phys.* **80**, 1083 (2008).
 - [13] M. Z. Hasan and C. L. Kane, Colloquium: Topological insulators, *Rev. Mod. Phys.* **82**, 3045 (2010).
 - [14] X.-L. Qi and S.-C. Zhang, Topological insulators and superconductors, *Rev. Mod. Phys.* **83**, 1057 (2011).
 - [15] J. Alicea, Y. Oreg, G. Refael, F. von Oppen, and M. P. A. Fisher, Non-abelian statistics and topological quantum information processing in 1d wire networks, *Nat. Phys.* **7**, 412 (2011).
 - [16] M. Leijnse and K. Flensberg, Introduction to topological superconductivity and majorana fermions, *Semicond. Sci. Technol.* **27**, 124003 (2012).
 - [17] Y. Ando, Topological insulator materials, *J. Phys. Soc. Jpn.* **82**, 102001 (2013).
 - [18] G. Tkachov and E. M. Hankiewicz, Spin-helical transport in normal and superconducting topological insulators, *Phys. Status Solidi B* **250**, 215 (2013).
 - [19] H.-J. Kwon, K. Sengupta, and V. M. Yakovenko, Fractional ac josephson effect in p- and d-wave superconductors, *Eur. Phys. J. B* **37**, 349 (2004).
 - [20] L. Fu and C. L. Kane, Superconducting proximity effect and majorana fermions at the surface of a topological insulator, *Phys. Rev. Lett.* **100**, 096407 (2008).
 - [21] L. Fu and C. L. Kane, Josephson current and noise at a superconductor/quantum-spin-hall-insulator/superconductor junction, *Phys. Rev. B* **79**, 161408 (2009).
 - [22] A. Keselman, L. Fu, A. Stern, and E. Berg, Inducing time-reversal-invariant topological superconductivity and fermion parity pumping in quantum wires, *Phys. Rev. Lett.* **111**, 116402 (2013).
 - [23] J. Li, W. Pan, B. A. Bernevig, and R. M. Lutchyn, Detection of majorana kramers pairs using a quantum point contact, *Phys. Rev. Lett.* **117**, 046804 (2016).
 - [24] B. Lu, P. Bursset, and Y. Tanaka, Spin-polarized multiple andreev reflections in spin-split superconductors, *Phys. Rev. B* **101**, 020502 (2020).
 - [25] T. Klapwijk, G. Blonder, and M. Tinkham, Explanation of subharmonic energy gap structure in superconducting contacts, *Physica B+C* **109-110**, 1657 (1982), 16th International Conference on Low Temperature Physics, Part 3.
 - [26] M. Octavio, M. Tinkham, G. E. Blonder, and T. M. Klapwijk, Subharmonic energy-gap structure in superconducting constrictions, *Phys. Rev. B* **27**, 6739 (1983).
 - [27] G. B. Arnold, Superconducting tunneling without the tunneling hamiltonian. ii. subgap harmonic structure, *J. Low. Temp. Phys.* **68**, 1 (1987).
 - [28] E. N. Bratus', V. S. Shumeiko, and G. Wendin, Theory of subharmonic gap structure in superconducting mesoscopic tunnel contacts, *Phys. Rev. Lett.* **74**, 2110 (1995).
 - [29] D. Averin and A. Bardas, ac josephson effect in a single quantum channel, *Phys. Rev. Lett.* **75**, 1831 (1995).
 - [30] J. C. Cuevas, A. Martín-Rodero, and A. L. Yeyati, Hamiltonian approach to the transport properties of superconducting quantum point contacts, *Phys. Rev. B* **54**, 7366 (1996).
 - [31] D. M. Badiane, M. Houzet, and J. S. Meyer, Nonequilibrium josephson effect through helical edge states, *Phys. Rev. Lett.* **107**, 177002 (2011).
 - [32] P. San-Jose, J. Cayao, E. Prada, and R. Aguado, Multiple andreev reflection and critical current in topological superconducting nanowire junctions, *New J. Phys.* **15**, 075019 (2013).
 - [33] A. Zazunov, R. Egger, and A. Levy Yeyati, Low-energy theory of transport in majorana wire junctions, *Phys. Rev. B* **94**, 014502 (2016).
 - [34] L. A. O. Olthof, S. R. de Wit, I. A. Shu-Ichiro Suzuki, J. W. Robinson, and A. Brinkman, [arXiv:2301.02270](https://arxiv.org/abs/2301.02270) (2023).
 - [35] M. Hurd, S. Datta, and P. F. Bagwell, ac josephson effect for asymmetric superconducting junctions, *Phys. Rev. B* **56**, 11232 (1997).
 - [36] B. Zhou, H.-Z. Lu, R.-L. Chu, S.-Q. Shen, and Q. Niu, Finite size effects on helical edge states in a quantum spin-hall system, *Phys. Rev. Lett.* **101**, 246807 (2008).
 - [37] G. E. Blonder, M. Tinkham, and T. M. Klapwijk, Transition from metallic to tunneling regimes in superconducting microconstrictions: Excess current, charge imbalance, and supercurrent conversion, *Phys. Rev. B* **25**, 4515 (1982).
 - [38] Y. Tanaka and S. Kashiwaya, Theory of tunneling spectroscopy of d -wave superconductors, *Phys. Rev. Lett.* **74**, 3451 (1995).
 - [39] K. Sengupta, I. Žutić, H.-J. Kwon, V. M. Yakovenko, and S. Das Sarma, Midgap edge states and pairing symmetry of quasi-one-dimensional organic superconductors, *Phys. Rev. B* **63**, 144531 (2001).
 - [40] C. J. Bolech and E. Demler, Observing majorana bound states in p -wave superconductors using noise measurements in tunneling experiments, *Phys. Rev. Lett.* **98**, 237002 (2007).
 - [41] A. R. Akhmerov, J. Nilsson, and C. W. J. Beenakker, Electrically detected interferometry of majorana fermions in a topological insulator, *Phys. Rev. Lett.* **102**, 216404 (2009).
 - [42] Y. Tanaka, T. Yokoyama, and N. Nagaosa, Manipulation of the majorana fermion, andreev reflection, and joseph-

- son current on topological insulators, *Phys. Rev. Lett.* **103**, 107002 (2009).
- [43] K. T. Law, P. A. Lee, and T. K. Ng, Majorana fermion induced resonant andreev reflection, *Phys. Rev. Lett.* **103**, 237001 (2009).
- [44] K. Flensberg, Tunneling characteristics of a chain of majorana bound states, *Phys. Rev. B* **82**, 180516 (2010).
- [45] F. Crépin, B. Trauzettel, and F. Dolcini, Signatures of Majorana bound states in transport properties of hybrid structures based on helical liquids, *Phys. Rev. B* **89**, 205115 (2014).
- [46] F. Crépin, P. Buset, and B. Trauzettel, Odd-frequency triplet superconductivity at the helical edge of a topological insulator, *Phys. Rev. B* **92**, 100507(R) (2015).
- [47] S. Ikegaya, Y. Asano, and Y. Tanaka, Anomalous proximity effect and theoretical design for its realization, *Phys. Rev. B* **91**, 174511 (2015).
- [48] S. Ikegaya, S.-I. Suzuki, Y. Tanaka, and Y. Asano, Quantization of conductance minimum and index theorem, *Phys. Rev. B* **94**, 054512 (2016).
- [49] B. Lu, P. Buset, Y. Tanuma, A. A. Golubov, Y. Asano, and Y. Tanaka, Influence of the impurity scattering on charge transport in unconventional superconductor junctions, *Phys. Rev. B* **94**, 014504 (2016).
- [50] P. Buset, B. Lu, S. Tamura, and Y. Tanaka, Current fluctuations in unconventional superconductor junctions with impurity scattering, *Phys. Rev. B* **95**, 224502 (2017).
- [51] F. Keidel, P. Buset, and B. Trauzettel, Tunable hybridization of majorana bound states at the quantum spin hall edge, *Phys. Rev. B* **97**, 075408 (2018).
- [52] C. Fleckenstein, F. Keidel, B. Trauzettel, and N. Traverso Ziani, The invisible majorana bound state at the helical edge, *Eur. Phys. J-spec. Top.* **227**, 1377 (2018).
- [53] C. Fleckenstein, N. Traverso Ziani, and B. Trauzettel, Conductance signatures of odd-frequency superconductivity in quantum spin Hall systems using a quantum point contact, *Phys. Rev. B* **97**, 134523 (2018).
- [54] J. Cayao and P. Buset, Confinement-induced zero-bias peaks in conventional superconductor hybrids, *Phys. Rev. B* **104**, 134507 (2021).
- [55] J. Cayao, P. Dutta, P. Buset, and A. M. Black-Schaffer, Phase-tunable electron transport assisted by odd-frequency cooper pairs in topological josephson junctions, *Phys. Rev. B* **106**, L100502 (2022).
- [56] B. Lu, G. Cheng, P. Buset, and Y. Tanaka, Identifying majorana bound states at quantum spin hall edges using a metallic probe, *Phys. Rev. B* **106**, 245427 (2022).
- [57] J. Lantz, V. S. Shumeiko, E. Bratus, and G. Wendin, Phase-dependent multiple andreev reflections in sns interferometers, *Phys. Rev. B* **65**, 134523 (2002).
- [58] A. V. Galaktionov, A. D. Zaikin, and L. S. Kuzmin, Andreev interferometer with three superconducting electrodes, *Phys. Rev. B* **85**, 224523 (2012).
- [59] R.-P. Riwar, D. M. Badiane, M. Houzet, J. S. Meyer, and Y. V. Nazarov, Cross-correlations of coherent multiple andreev reflections, *Physica E* **76**, 231 (2016).
- [60] M. P. Nowak, M. Wimmer, and A. R. Akhmerov, Super-current carried by nonequilibrium quasiparticles in a multi-terminal josephson junction, *Phys. Rev. B* **99**, 075416 (2019).
- [61] S. Hart, H. Ren, T. Wagner, P. Leubner, M. Mühlbauer, C. Brüne, H. Buhmann, L. W. Molenkamp, and A. Yacoby, Induced superconductivity in the quantum spin Hall edge, *Nat. Phys.* **10**, 638 (2014).
- [62] V. S. Pribiag, A. J. A. Beukman, F. Qu, M. C. Cassidy, C. Charpentier, W. Wegscheider, and L. P. Kouwenhoven, Edge-mode superconductivity in a two-dimensional topological insulator, *Nat. Nanotechnol.* **10**, 593 (2015).
- [63] E. Bocquillon, R. S. Deacon, J. Wiedenmann, P. Leubner, T. M. Klapwijk, C. Brüne, K. Ishibashi, H. Buhmann, and L. W. Molenkamp, Gapless Andreev bound states in the quantum spin Hall insulator HgTe, *Nat. Nanotechnol.* **12**, 137 (2017).
- [64] H. Ren, F. Pientka, S. Hart, A. T. Pierce, M. Kosowsky, L. Lunczer, R. Schlereth, B. Scharf, E. M. Hankiewicz, L. W. Molenkamp, B. I. Halperin, and A. Yacoby, Topological superconductivity in a phase-controlled josephson junction, *Nature* **569**, 93 (2019).
- [65] A. Fornieri, A. M. Whiticar, F. Setiawan, E. Portolés, A. C. C. Drachmann, A. Keselman, S. Gronin, C. Thomas, T. Wang, R. Kallaher, G. C. Gardner, E. Berg, M. J. Manfra, A. Stern, C. M. Marcus, and F. Nichele, Evidence of topological superconductivity in planar josephson junctions, *Nature* **569**, 89 (2019).